Use of a CCD diffractometer in crystal structure determinations at high pressure

Journal of
Applied Crystallography
ISSN 0021-8898

Received 25 October 2003
Accepted 25 March 2004

Use of a CCD diffractometer in crystal structure determinations at high pressure

Alice Dawson,[a] David R. Allan,[a] Simon Parsons[a]* and Michael Ruf[b]

[a]School of Chemistry and Centre for Science at Extreme Conditions, The University of Edinburgh, King's Buildings, West Mains Road, Edinburgh EH9 3JJ, Scotland, and [b]Bruker–Nonius Inc., 5465 East Cheryl Parkway, Madison, WI 53711, USA. Correspondence e-mail: s.parsons@ed.ac.uk

Although CCD instruments are now widely used in single-crystal diffraction, they have not been employed so extensively in crystallographic studies at high pressure. This paper describes some practical experience in the application of one CCD instrument, the Bruker–Nonius SMART APEX (a fixed-χ instrument). Centring a sample in a pressure cell is complicated by the restrictions on viewing the sample imposed by the body of the cell. The data collection strategy is defined by the requirements that (i) the incident beam must illuminate the sample and (ii) no more than 80% of the detector should be shaded by the body of the pressure cell. High-pressure diffraction images are contaminated by powder lines from the gasket and backing-disk materials, which form part of the pressure cell, and very intense spots from the diamond anvils. Procedures for the selection of spots for indexing are described. Integration routines attempt to harvest intensity data from regions of the detector that are shaded by the body of the pressure cell, and a procedure for generating dynamic masks is described. Shading also reduces the volume of reciprocal space that can be sampled, although this can be increased by performing data collections at more than one pressure-cell setting. Corrections for absorption are carried out in a two-stage procedure comprising an analytical correction for absorption by the cell, followed by a second multi-scan correction. Data sets collected at high pressure often contain some significant outliers; these can be identified during merging using a robust resistant weighting scheme, as described by Blessing [*J. Appl. Cryst.* (1997), **30**, 421–426].

1. Introduction

Although the majority of single-crystal diffraction studies at high pressure have been performed using four-circle diffractometers with point detectors, data collection times may run into weeks, especially for relatively weakly diffracting organic samples with low-symmetry crystal systems and unit-cell volumes in excess of 1000 Å^3. This area has recently been the subject of a series of reviews (Angel *et al.*, 2000; Hemley & Dera, 2000; Miletich *et al.*, 2000). There are clear potential advantages in the use of area detectors for this work. CCD diffractometers are now used ubiquitously in chemical crystallography, and in this paper we describe some practical experience in the application of one such instrument, a Bruker–Nonius SMART APEX diffractometer, in high-pressure diffraction.

The SMART consists of an X-ray source, a CCD detector and a three-circle goniometer. The detector can move around 2θ, and the sample can be oriented about ω and φ, but χ is fixed at 54.76°. The advantage of this very open arrangement is that it can accommodate bulky sample environments, such as various designs of high-pressure cell. The Merrill–Bassett diamond-anvil cell (DAC; Merrill & Bassett, 1974) is one of the most widely used high-pressure devices. It is suitable for obtaining pressures up to 12 GPa. Its compact size means that it can be mounted on a standard goniometer head.

Centring the sample may be difficult because of the restrictions on viewing by the body of the pressure cell; procedures such as eight-point centring (Angel *et al.*, 2000) cannot be used on fixed-χ instruments. Diffraction images contain not only sample spots but also powder lines from the gasket and backing-disk materials and very intense spots from the diamond anvils (Fig. 1). The result is a high and variable background, which can present problems during indexing and unit-cell determination. Shading of the detector by the body of the pressure cell means that only a restricted volume of reciprocal space can be sampled, and this results in very low data completeness for samples in the triclinic and monoclinic crystal systems. The lack of a χ-circle on the SMART potentially exacerbates this problem. The high background and

shading also introduce problems during integration. After integration, the absorption correction needs to take into account not only sample anisotropy but also absorption by the diamonds and backing disks. The aim of the present paper is to describe some procedures by which these difficulties can be addressed.

2. Experimental

2.1. General details and procedures

Acetic acid was chosen as a test system for this study. Glacial acetic acid was obtained from Aldrich and used as received. After being loaded as a liquid into the pressure cell, the acetic acid was crystallized according to the procedure described by Allan & Clark (1999). The pressure was found to be 0.46 GPa using the ruby fluorescence method.

With the exception of cell-transmission measurements, which were carried out using a procedure based on that described by Finger & King (1978) on a CAD-4 diffractometer, all data collections were performed at room temperature on a Bruker SMART APEX diffractometer, with graphite-monochromated Mo $K\alpha$ radiation from a conventional sealed-tube source operating at 2 kW. A few modifications to the diffractometer were necessary to allow high-pressure data to be collected. To generate more space for movement of the diamond-anvil cell, the standard collimator (17.3 cm) was replaced by a locally fabricated short collimator (12.3 cm). Also, for reasons of maximizing space around the sample and for the purpose of centring the sample (see below), a beam stop was not used and during data collection the detector positioned so that the direct beam did not impinge on it.

Merrill–Bassett diamond-anvil cells were manufactured locally with 400 μm culet diamonds, 1.3 cm-diameter beryllium backing disks (Diacell Products) and 250 mm tungsten foil (Aldrich) as a gasket (Fig. 2). The cell was 'superglued' to a small metal platform designed to fit into a standard goniometer head.

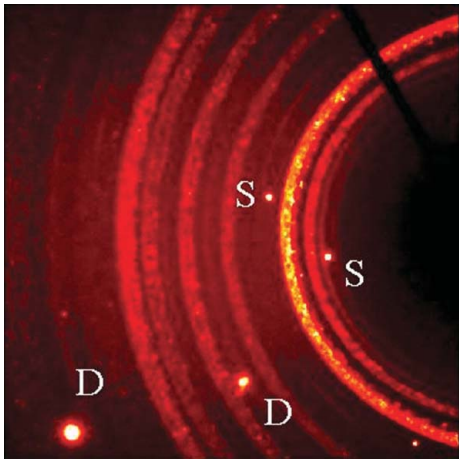

Figure 1
A typical data collection frame taken with a Merrill–Bassett diamond-anvil cell. Reflections from the sample are labelled 'S', those from the diamonds, 'D'. The powder rings derive from the Be backing disks (see Fig. 2).

2.2. Sample centring

When a sample is contained in a Merrill–Bassett cell it can only be viewed along the direction parallel to the cell axis through the diamond anvils. Optical centring of the sample in the two orthogonal directions perpendicular to this is relatively straightforward, although it is important to ensure that the cell axis is aligned coaxially with the line of view. Let φ_0 be the value of φ for which the cell axis is parallel to the direct beam at $\omega = 0^\circ$; this arrangement can be achieved by aligning the cell face against a machine square that is conveniently placed on the base plate of the instrument.

Accurate optical centring along the cell axis is not possible because the sample is obscured by the gasket. Centring in this direction is achieved by a three-stage procedure. Initially, centring the edge of the gasket acts to centre the sample approximately. The cell is then rotated so that the line of view is through the diamond anvils. The video camera, used for viewing the sample, is mounted on an adjustable platform fitted with a micrometer; the camera is first focused on the sample with $\varphi = \varphi_0$, and the micrometer reading is noted. The cell is then rotated to $\varphi = \varphi_0 + 180^\circ$, the camera is refocused on the sample and the new micrometer reading is noted. The video camera is then moved to the mid-point of the two micrometer readings and the position of the cell adjusted so as to re-establish a focused image of the sample. This procedure is then repeated until the sample is in focus with the cell in both settings of φ.

A final check on the centring of the sample in the direction of the cell axis was first suggested to us by Meyer (2002). An image of the direct beam is acquired on the CCD detector with the X-ray generator set at low power (30 kV and 10 mA), the detector at $2\theta = 0^\circ$, and the sample at some non-zero value of ω (typically 25°) and $\varphi = \varphi_0$. A second image with the sample at $-\omega$ (-25°) is then acquired, and the images are subtracted. If the cell is correctly centred, the pixel values in the subtracted image at the position of the direct beam should be

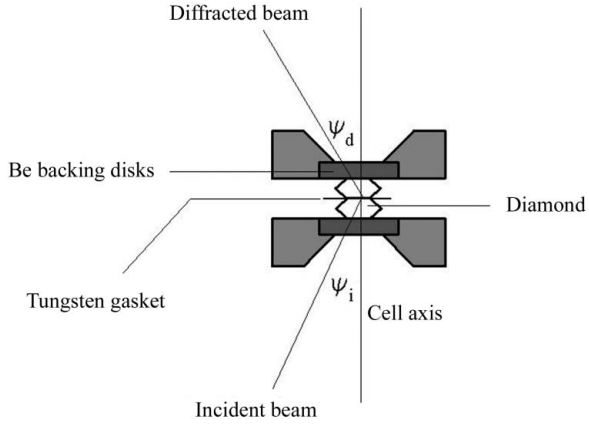

Figure 2
A schematic representation of a section through a Merrill–Bassett diamond-anvil cell, showing the definition of the cell axis.

Table 1
Summary of a high-pressure data collection strategy assuming a Merrill–Bassett cell with an opening half-angle of 40°.

φ_0 (see §2.2) is assumed to be 90°. Exact ranges of ω vary with cell design. The limiting values of ω–2θ are 20.5 and −200.5°, although we usually avoid approaching these within ∼2°. The ω range is defined by the requirements that (i) the incident beam must illuminate the sample, and thus the angle between the incident beam and the cell axis should be no more than 40°, and (ii) no more than 80% of the detector should be shaded.

Run	2θ (°)	φ (°)	Range of ω (°)
1	−28	90	−10 to −40
2	28	90	40 to −25
3	−28	90	−155 to −220
4	28	90	−140 to −170
5	−28	270	−155 to −220
6	28	270	−140 to −170
7	−28	270	−10 to −40
8	28	270	40 to −25

zero. Miscentring along the axis of the pressure cell is therefore readily detected, and small adjustments to the centring can be made to remedy the situation. Miscentring of the gasket hole in the other translation axes of the goniometer head can be checked if necessary with direct-beam images taken at $\omega = 0°$ and $\varphi = \varphi_0$ and $\varphi_0 + 180°$, and then at $\omega = 0°$, $\varphi = \varphi_0$ and $\omega = 180°$, $\varphi = \varphi_0 + 180°$.

Another procedure for centring, based on diffractometric measurements, has been described by Dera & Katrusiak (1999).

2.3. Data collection strategy

Diffraction data can only be acquired at limited values of ω and φ, because the pressure cell body completely obscures the sample from the X-ray beam or the detector in certain orientations. Data were collected in steps of ω in a series of eight settings of 2θ and φ, in which the detector was set to $2\theta = \pm 28°$ with two settings of φ (φ_0 and $\varphi_0 + 180°$). A typical data collection sequence is shown in Table 1. Data completeness can be enhanced if the sequence shown in Table 1 is carried out at several different settings of χ. Since the SMART APEX has χ fixed at 54.75°, this situation can be simulated by re-collecting data with the pressure cell attached to the goniometer head on each of its three sides. The completeness (to 0.9 Å) of each single run was between 48 and 54%, but increased to 60% when data from the three collections were combined. Each data set was integrated and treated for absorption separately, and the three data sets were then scaled and merged (see below).

2.4. Indexing

Determination of the orientation matrix was not attempted until data collection had been completed. The diffraction pattern obtained from a sample in a high-pressure cell contains not only sample peaks but also λ and λ/2 reflections from the diamonds and the powder rings from the beryllium backing disks. 'Default' indexing procedures often fail to index the diffraction pattern and use of a program designed for twinned samples is usually necessary. In other high-pressure diffraction studies, we have found that automatic peak finding yields a set of reflections that can be indexed (provided that reflections from the beryllium powder rings are excluded), but this was not the case for the sample of acetic acid used in this work. Where automatic procedures fail, manual harvesting of reflections frequently results in a list of reflections that can be indexed; for example, out of 49 reflections selected from runs 1 and 2 of one data collection (see Table 1), 31 were indexed (*GEMINI*; Sparks, 2000) on the basis of the acetic acid unit cell. The orientation matrix was then refined, but the limited range of data used to index the sample meant that the matrix was inaccurate and imprecise. It was improved by integrating all the runs using the program *SAINT* (Bruker, 2003) and using the positions of all intense reflections in the data set in a constrained cell refinement.

2.5. Integration

The data set was integrated (*SAINT*) using box-size parameters derived from the observed profile of the peaks in the diffraction pattern. These were not allowed to optimize during integration. The orientation matrix, which had been refined in a previous integration run (see above), was not allowed to refine further.

A mask was generated for each diffraction image so that pixels shaded by the pressure cell were not integrated. A shaded pixel was identified by evaluating the angle subtended by a vector **D** drawn from the crystal to the pixel in question and the vector **C** passing through the sample perpendicular to the diamond culets and backing disks (the cell axis). It is convenient to carry out this calculation in the laboratory axis system, with basis vectors ($\mathbf{X}_L$, $\mathbf{Y}_L$, $\mathbf{Z}_L$). On the SMART diffractometer, $\mathbf{X}_L$ points along the forward direction of the X-ray beam, $\mathbf{Z}_L$ is vertical, pointing up, and $\mathbf{Y}_L$ completes a right-handed set (Fig. 3). Images on the SMART are read in 'frames' of 512 × 512 pixels, with pixel [0, 0] at the bottom left of the detector and the pixel with coordinates [511, 511] at the top right. When $2\theta = 0°$, the detector x axis is parallel to $-\mathbf{Y}_L$ and the detector y axis is parallel to $+\mathbf{Z}_L$.

Consider a pixel with coordinates $[x, y]$ on the detector, which is positioned at $2\theta = 0°$; the crystal–detector distance is d (mm). The coordinates of this point in millimetres, referred to an origin at the centre of the detector face, are $[x_{mm}, y_{mm}] = [p(x - x_{centre}), p(y - y_{centre})]$, where p is the pixel size in millimetres and (x_{centre}, y_{centre}) are the pixel coordinates of the point at which the direct X-ray beam hits the detector when $2\theta = 0°$. In the laboratory frame, the vector **D** describing the position of the pixel is therefore

$$\mathbf{D} = \begin{bmatrix} d \\ -p(x - x_{centre}) \\ p(y - y_{centre}) \end{bmatrix}.$$

If the detector is at some swing angle 2θ, **D** becomes

$$\mathbf{D} = \begin{bmatrix} \cos 2\theta & -\sin 2\theta & 0 \\ \sin 2\theta & \cos 2\theta & 0 \\ 0 & 0 & 1 \end{bmatrix} \begin{bmatrix} d \\ -p(x - x_{centre}) \\ p(y - y_{centre}) \end{bmatrix}.$$

Consider a unit vector **C**, lying along the pressure-cell axis. If the cell is mounted on the goniometer so that the cell axis points along $+\mathbf{X}_L$ when $\omega = 0$,

$$\mathbf{C} = \begin{pmatrix} 1 \\ 0 \\ 0 \end{pmatrix}.$$

As the cell is rotated about ω, **C** becomes

$$\mathbf{C} = \begin{pmatrix} \cos\omega & -\sin\omega & 0 \\ \sin\omega & \cos\omega & 0 \\ 0 & 0 & 1 \end{pmatrix} \begin{pmatrix} 1 \\ 0 \\ 0 \end{pmatrix}.$$

The angle between **C** and **D** is calculated from the dot-product $\mathbf{C}\cdot\mathbf{D}$. If the angle is greater than the half opening angle of the cell (40° in our case), the pixel is considered to be shaded and the pixel mask is given a value of 0. Unshaded pixels have a mask value of 64 (Fig. 4). Since the SMART APEX detector does not use a magnification glass taper, no spatial correction was required and no further calculation was necessary to generate the mask files.

2.6. Absorption correction and merging

Absorption by the pressure cell was treated according to the method described by Finger & King (1978); gasket-shading was treated in the manner described by Von Dreele & Hanson (1984). Reflections where the incident or diffracted beams lay within 2° of the DAC half-angle cut-off (40°) were not included in the data set if they had poor profile correlation coefficients (< 0.3). These calculations were carried out using a locally written program (*SHADE*; Parsons, 2004); the angles between the cell axis and the incident and diffracted beams were calculated according to Allan *et al.* (2000). Additional systematic errors were corrected using the multi-scan correction program *SADABS* (Sheldrick, 2004). The results of these three procedures, and some combinations of them, are compared in Table 2. The data were merged using *SORTAV* (Blessing, 1997) [as incorporated into *WinGX* (Farrugia, 1999)], and details are given in the caption to Table 2. After data merging, Bayesian estimates of F_o^2 and $\sigma(F_o^2)$ were obtained using the method of French & Wilson (1978) as incorporated into *SORTAV*.

2.7. Refinement

Refinement was carried out using the previously determined structure for the high-pressure phase of acetic acid (Allan & Clark, 1999). Refinements were against $|F|^2$, using all data to 0.9 Å (*CRYSTALS*; Betteridge *et al.*, 2003). The weighting scheme applied was

$$w = 1/[\sigma^2(F^2) + (aP)^2 + bP],$$

where

$$P = \mathrm{MAX}(F_o^2, 0)/3 + 2F_c^2/3$$

and a and b are adjustable parameters (Sheldrick, 1993). The program enables a robust resistant modifier (Prince & Nicholson, 1983) to be applied to weights, although the results of the procedure were, in this case, almost indistinguishable from those obtained with unmodified weights. H-atom positions were refined subject to restraints such that the methyl group had local threefold symmetry, the O—H bond distance was 0.81 (1) Å and the C—O—H angle was 109 (1)°. All other parameters, including anisotropic displacement parameters of the C and O atoms, were refined freely. The total number of parameters was 50. Displacement ellipsoid plots showing the molecular structure of acetic acid are shown in Fig. 5; distances and angles are given in Table 3, where they are compared with those derived by Boese *et al.* (1999) in the low-temperature phase at 40 K. Structural and reflection data are available as supplementary data in CIF format.[1]

Table 2
Comparison of absorption correction and merging strategies for refinement of the crystal structure of acetic acid at 0.46 GPa.

The correction for absorption by the beryllium and diamond components of the pressure cell (DAC) was described by Finger & King (1978); the gasket correction used the method of Von Dreele & Hanson (1984). The multi-scan correction was carried out using *SADABS* (Sheldrick, 2004); the maximum even- and odd-order spherical harmonics were 4 and 1, respectively. Merging was carried out with the program *SORTAV*, using what Blessing (1997) describes as 'experimental weights'; this scheme was used in preference to unit weighting because data from three different data collections were being merged. Robust resistant outlier down-weighting or rejection was used for all methods except number 5. Blessing's z_{max} parameter was set to 6. All refinements were carried out against F^2 for all data, but R factors quoted here are unweighted and calculated using F.

Correction method	R_{int}	$R(F$, all data)	$R[F > 4\sigma(F)]$	No. of observations/all
1. No corrections	10.13	7.83	5.80	178/249
2. DAC + gasket only	8.85	6.21	4.01	182/249
3. Multi-scan only	6.75	6.06	3.96	189/249
4. DAC + gasket + multi-scan	5.96	5.86	3.79	189/249
5. As 4, but no outlier rejection during merging	6.35	6.04	3.89	186/249

Table 3
Bond distances and angles in acetic acid at 0.46 GPa and 298 K, and at ambient pressure and 40 K.

Bond/angle (Å, °)	0.46 GPa (this work)	40 K (Boese *et al.* 1999)
C1—O1	1.312 (3)	1.3208 (16)
C1—O2	1.205 (3)	1.2156 (16)
C1—C2	1.491 (4)	1.4903 (18)
O1—C1—O2	122.1 (3)	121.90 (13)
O1—C1—C2	113.2 (3)	113.51 (11)
O2—C1—C2	124.7 (3)	124.59 (12)

3. Discussion

This paper describes a case study in which the crystal structure of acetic acid at high pressure was determined using data collected using a CCD area detector. The advantage of using a liquid crystallized *in situ* under pressure is that this avoids

[1] Supplementary data for this paper are available from the IUCr electronic archives (Reference: HE5280). Services for accessing these data are described at the back of the journal.

pressure-induced peak broadening that may occur when pressure is applied to a crystal obtained under ambient conditions. Procedures for data collection and indexing are described in the experimental section.

3.1. Data collection

The data collection strategy outlined in Table 1 is used for all data collections in our laboratory. In the case of the acetic acid sample used here, 477 reflections with different values of h, k and l were measured to 0.9 Å, corresponding to 29% of the total number of reflections available (1665). The proportion theoretically accessible is 39% (Merrill & Bassett, 1974, equation 8), rather larger than that obtained here. The sampling would be increased with full four-circle capability; during some recent tests carried out as part of an instrument-purchasing exercise using a sample of pyrimidine, we observed values of between 30 and 35% on instruments from different manufacturers. Of more importance, however, is the completeness in terms of symmetry-independent reflections, and this value is also determined by the orientation of the

(*a*)

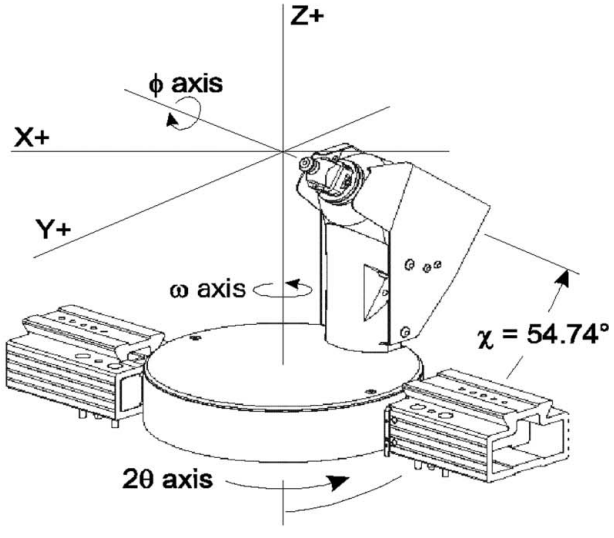

(*b*)

Figure 3
Views of (*a*) the instrument and (*b*) the axis system. The low-temperature device [the nozel of which is visible in the top part of (*a*)] was not used for the experiments described here.

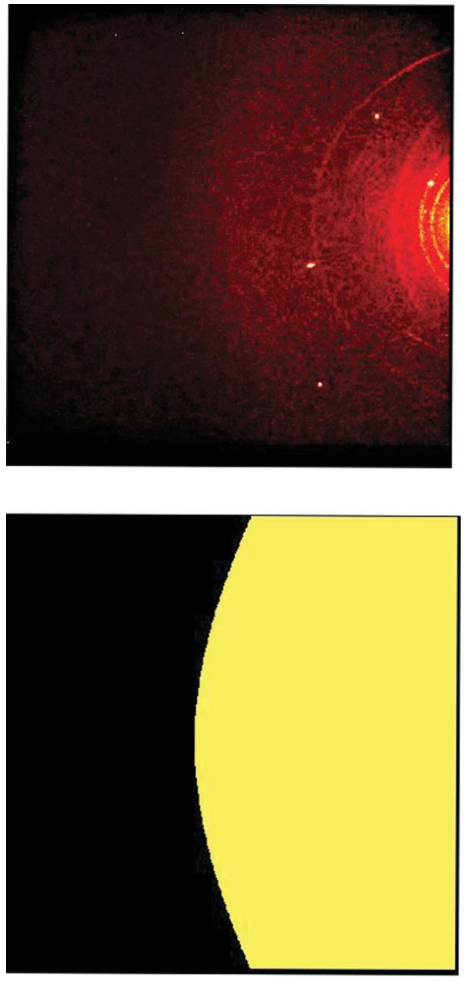

Figure 4
Most data collection frames are shaded by the steel support components of the pressure cell. These regions are excluded from the integration by means of dynamic masks. A partially shaded frame (top) and its corresponding mask (bottom) are shown. The masked region is black. Note that, in contrast to the frame shown in Fig. 1, the cell was at such an angle that the incident beam did not pass through a Be backing disk; therefore, no Be powder lines are observed. The narrow powder lines on this image derive from the tungsten gasket.

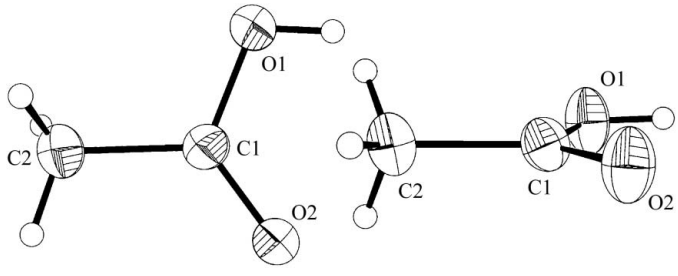

Figure 5
The molecular structure of acetic acid at 0.46 GPa and 298 K. Ellipsoids enclose 30% probability surfaces; H atoms are drawn as circles of arbitrary radii (*XP*; Sheldrick, 2001).

crystal in the pressure cell. The completeness obtained here was 60%, and this is comparable with studies of monoclinic crystals carried out on four-circle instruments (*e.g.* Allan & Clark, 1999; Boldyreva *et al.*, 2000). Furthermore, these data were collected in a fraction of the time (24 h) needed to collect a similar data set on a four-circle diffractometer. Procedures used for indexing are described in the experimental section.

3.2. Integration

Contamination of the diffraction pattern by scattering from the beryllium backing disks and the diamonds, combined with shading of the detector by the body of the pressure cell, present certain difficulties during integration. The two principal issues to be addressed are (i) rejection of data from regions of the detector shaded by the pressure cell and (ii) choice of parameters for integration. Of course, a well determined orientation matrix is essential for successful integration.

As the data collection proceeds, different areas of the detector become shaded by the body of the cell, and the integration should avoid these regions (Fig. 4). The need to optimize both redundancy and data-set completeness means that it is still necessary to harvest sample diffraction peaks even from images where the majority of the detector area was obscured by the cell. If a data set is integrated normally, *i.e.* without regard to shading, the output contains reflections harvested from shaded regions of the detector. We have previously described a procedure (Allan *et al.*, 2000) by which such reflections can be identified and omitted from a data set, which may then be corrected for absorption, merged and used for refinement. Although this procedure yields data sets suitable for structure analysis, the diagnostic output of the integration listing is next to worthless because 'data' harvested from shaded regions contribute to profile and merging statistics.

Masking of detector regions during integration is a well established means of avoiding areas of the detector shaded by hardware items, such as the beam stop, during integration. In general, such masks are 'static', that is, the same mask can be used during processing of a whole series of diffraction images. This procedure would not be appropriate for a data collection with a high-pressure cell, because the shaded region is different for each image. Instead, a series of masks were calculated that modelled the changing orientation of the cell with respect to the detector. Each image therefore had its own mask file; this process is known as 'dynamic masking'.

In the procedure currently implemented, the angle subtended by the cell axis and a vector from the centre of the cell to a pixel on the detector is calculated. If this angle is greater than half the opening angle of the cell (typically 40°), the pixel is shaded. This calculation is performed for every pixel on the detector in every diffraction image. Mask generation takes about 20 min on a 2.2 GHz PC with a Pentium IV processor; integration then usually takes a further 5–10 min. A computationally more efficient procedure would be to perform this calculation 'on the fly' during integration, although the same set of masks can be used repeatedly for experiments carried out with the same data collection strategy. However, what is lost in computational efficiency is gained in flexibility; it is a simple matter to adapt the computer code used for these calculations to mask any feature. We have recently found this method to be useful for masking the very intense Be diffraction rings obtained with synchrotron radiation.

The quality of a structure refinement can be influenced by choice of integration parameters, particularly box size. We typically carry out at least one integration in order to optimize the orientation matrix for the whole data collection; this matrix is then used in a subsequent cycle of integration. Automatic procedures for optimizing integration parameters that work well for ambient pressure data collections are less successful in high-pressure work. Automatic box-size optimization can fail because of the presence in the diffraction pattern of a high background and beryllium rings. The optimization may also be imprecise when only a few reflections are available because the material being studied has a small unit cell. In most cases, it is preferable to obtain an estimate of the box size directly from the data-collection images and hold it constant during integration. The box size may be increased or decreased manually after inspection of the integration statistics, such as plots of the average peak profile.

3.3. Absorption corrections and merging

Several methods for calculating an absorption correction and merging the data were tested, and the results are summarized in Table 2. Although refinements were carried out *versus* $|F|^2$, we have chosen to compare refinements of the unweighted R factor calculated on $|F|$ using all data. In contrast to the weighted residual wR_2, this parameter is not sensitive to the numerical values used for the weights. With a small data set, the conventional R factor calculated on $|F|$ using data with $|F| > 4\sigma(|F|)$ can vary as a result of the differing σ values output by different programs.

Systematic absorption errors in data sets collected at high pressure arise not only from the sample but also because of variation of the beam path through the beryllium backing disks and the diamonds of the pressure cell and because of shading by the gasket hole. The methods used to correct for the second and third of these are described in §2. Reference to Table 2 (rows 1 and 2) shows that application of these corrections leads to an improvement in R of 1.6% over uncorrected data.

Other systematic errors can arise from deviations from assumptions made in the gasket correction procedure, absorption by the sample, crystal decay, direct beam intensity dips due to diamond reflections, *etc*. Multi-scan absorption corrections, which exploit the high redundancy of data sets collected with area detectors, are now well established and provide a means of correcting for any systematic error that leads to variations in the intensities of ψ-equivalent reflections. The programs *SADABS* (Sheldrick, 2004) and *SORTAV* (Blessing, 1995) use spherical harmonic functions to model absorption anisotropy and other systematic errors. Although

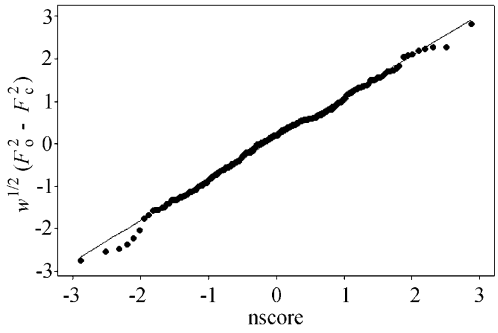

Figure 6
A normal probability plot showing 249 values of observed values of $w^{1/2}(|F_o| - |F_c|)$ for the refinement of the crystal structure of acetic acid at 0.46 GPa against their normal scores (nscore). These data derive from the refinement in row 4 of Table 2. The equation of the line is $w^{1/2}(|F_o|^2 - |F_c|^2) = 0.129 + 0.970$nscore.

the completeness of data sets collected using high-pressure cells is low, redundancy is generally adequate for multi-scan methods. An effective absorption correction was obtained by multi-scan procedures alone (Table 2, row 3), although the best statistics were obtained by a combination of the DAC and multi-scan corrections (Table 2, row 4).

In spite of the corrections described above, data collected using pressure cells still suffer from substantial systematic errors. These arise, for example, from overlap of reflections with beryllium powder rings, but a few reflections may be wildly in error if they overlap with reflections from the diamonds. Blessing (1997) has described how the effect of outlying data can be treated in a controlled way using a robust resistant weighting scheme, and this procedure is available in the program *SORTAV*. Our experience is that use of robust resistant weights in merging yields superior results to simple unit or reciprocal variance weights (compare Table 2, rows 4 and 5). Use of robust resistant weight modifiers during refinement is also an important tool in high-pressure crystallography if the data are still subject to errors, and this has been discussed in some detail by Prince & Nicholson (1983) and more recently by Angel *et al.* (2000). It was not necessary to apply these procedures in this study, however.

4. Conclusions

Data collection with a diamond-anvil cell on a CCD-based instrument and a three-circle goniometer has been shown to yield high-quality data, giving *R* factors comparable with those obtained under ambient conditions. Although the data are subject to substantial systematic errors, the normal probability plot (Abrahams & Keve, 1971), obtained from the refinement in row 4 of Table 2 and shown in Fig. 6, is linear and intersects near the origin, confirming that these errors have been effectively removed by the procedures described above. The refined displacement ellipsoids do not show any abnormal elongation (Fig. 4), which also attests to the quality of the data set. The refined bond distances and angles are the same within the standard uncertainties as those observed at 40 K and ambient pressure (Table 3) by Boese *et al.* (1999). This similarity is not unexpected; at pressures of the order of <1 GPa, structural effects tend to be observed in 'softer' torsion angles and intermolecular interactions such as hydrogen bonds; the latter have been discussed in an earlier paper (Allan & Clark, 1999). The standard uncertainties of the bond distances and angles are normal for a system of this type, though they are about twice as great as those obtained by Boese and co-workers, reflecting the higher resolution and completeness of their low-temperature data set.

The authors thank the EPSRC, The Royal Society, The Woolfson Foundation and The University of Edinburgh for financial support, and Dr M. Meyer (Oxford Diffraction) for pointing out the method described here for checking sample centring with the direct X-ray beam.

References

Abrahams, S. C. & Keve, E. T. (1971). *Acta Cryst.* A**27**, 157–165.
Allan, D. R. & Clark, S. J. (1999). *Phys. Rev. B*, **60**, 6328–6334.
Allan, D. R., Clark, S. J., Parsons, S. & Ruf, M. (2000). *J. Phys. Condens. Matter*, **12**, L613–L618.
Angel, R. J., Downs, R. T. & Finger, L. W. (2000). *Rev. Mineral. Geochem.* **41**, 559–596.
Betteridge, P. W., Carruthers, J. R., Cooper, R. I., Prout, K. & Watkin, D. J. (2003). *J. Appl. Cryst.* **36**, 1487.
Blessing, R. H. (1995). *Acta Cryst.* A**51**, 33–38.
Blessing, R. H. (1997). *J. Appl. Cryst.* **30**, 421–426.
Boese, R., Blaser, D., Latz, R. & Baumen, A. (1999). *Acta Cryst.* C**55**, 9900001.
Boldyreva, E. V., Shakhtshneider, T. P., Vasilchenko, M. A., Ahsbahs, H. & Uchtmann, H. (2000). *Acta Cryst.* B**56**, 299–300.
Bruker (2003). *SAINT*. Version 7.01A. Bruker AXS Inc., Madison, Wisconsin, USA.
Dera, P. & Katrusiak, A. (1999). *J. Appl. Cryst.* **32**, 510–515.
Farrugia, L. J. (1999). *J. Appl. Cryst.* **32**, 837–838.
Finger, L. W. & King, H. (1978). *Am. Mineral.* **63**, 337–342.
French, S. & Wilson, K. (1978). *Acta Cryst.* A**34**, 517–525.
Hemley, R. J. & Dera, P. (2000). *Rev. Mineral. Geochem.* **41**, 335–419.
Merrill, L. & Bassett, W. A. (1974). *Rev. Sci. Instrum.* **45**, 290–294.
Meyer, M. (2002). *Private Communication.*
Miletich, R., Allan, D. R. & Kuhs, W. F. (2000). *Rev. Mineral. Geochem.* **41**, 445–519.
Parsons, S. (2004). *SHADE*. The University of Edinburgh, Scotland.
Prince, E. & Nicholson, W. L. (1983). *Acta Cryst.* A**39**, 407–410.
Sheldrick, G. M. (1993). *SHELXL*93. University of Göttingen, Germany.
Sheldrick, G. M. (2001). *XP*. Version 6. University of Göttingen, Germany.
Sheldrick, G. M. (2004). *SADABS*. Version 2004/1. University of Göttingen, Germany.
Sparks, R. A. (2000). *GEMINI*. Version 1.05. Bruker AXS Inc., Madison, Wisconsin, USA.
Von Dreele, R. B. & Hanson, R. C. (1984). *Acta Cryst.* C**40**, 1635–1638.